

## Toward Low-Temperature Dehydrogenation Catalysis: Isophorone Adsorbed on Pd(111)

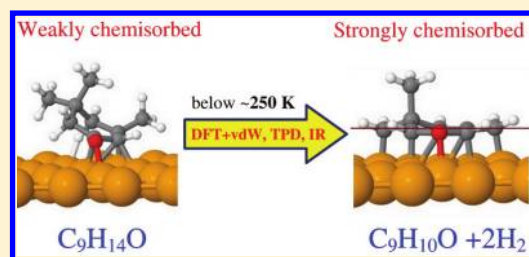
Wei Liu, Aditya Savara, Xinguo Ren, Wiebke Ludwig, Karl-Heinz Dostert, Swetlana Schauerma<sup>\*</sup>, Alexandre Tkatchenko,<sup>\*</sup> Hans-Joachim Freund, and Matthias Scheffler

Fritz-Haber-Institut der Max-Planck-Gesellschaft, Faradayweg 4-6, D-14195, Berlin, Germany

### S Supporting Information

**ABSTRACT:** Adsorbate geometry and reaction dynamics play essential roles in catalytic processes at surfaces. Here we present a theoretical and experimental study for a model functional organic/metal interface: isophorone ( $C_9H_{14}O$ ) adsorbed on the Pd(111) surface. Density functional theory calculations with the Perdew–Burke–Ernzerhoff (PBE) functional including van der Waals (vdW) interactions, in combination with infrared spectroscopy and temperature-programmed desorption (TPD) experiments, reveal the reaction pathway between the weakly chemisorbed reactant ( $C_9H_{14}O$ ) and the strongly chemisorbed product ( $C_9H_{10}O$ ), which occurs by the cleavage of four C–H bonds below 250 K. Analysis of the TPD spectrum is consistent with the relatively small magnitude of the activation barrier derived from PBE+vdW calculations, demonstrating the feasibility of low-temperature dehydrogenation.

**SECTION:** Surfaces, Interfaces, Catalysis



Heterogeneous catalysis plays an essential role in the chemical processing industry for production of pharmaceuticals and clean energy technologies.<sup>1</sup> Conversion of unsaturated hydrocarbons on transition metals is of immense practical importance because it provides large-scale manufacturing of valuable intermediates for many chemical processes. These types of reactions were extensively investigated in the early years using conventional catalytic techniques<sup>1,2</sup> and more recently by modern surface science methodologies.<sup>3–7</sup> To design the next generation of heterogeneous catalysts, it is necessary to understand the adsorption and chemistry of molecules which are versatile enough to display complex functionality. Here we choose the adsorption of isophorone (3,5,5-trimethyl-2-cyclohexen-1-one) on the Pd(111) surface as a prototypical model to study the mechanisms that govern the adsorption dynamics of organic/metal interfaces. Isophorone is an important proxy for catalysis because it contains conjugated C=C and C=O bonds that can be selectively hydrogenated. Isophorone is also a prochiral molecule that can be transformed to two enantiomers after selective hydrogenation of the olefinic double bond.<sup>8</sup>

Here we present density functional theory (DFT) calculations including van der Waals interactions (vdW), in combination with infrared (IR) spectroscopy and temperature-programmed desorption (TPD) experiments to reveal the reaction pathway from the weakly chemisorbed  $C_9H_{14}O$  reactant to the strongly chemisorbed  $C_9H_{10}O$  product after four C–H bond cleavages. Both the experimental TPD data and the relatively small magnitude of the activation barrier derived from DFT+vdW calculations support the feasibility of low-temperature dehydrogenation process. Our study illustrates

the feasibility of understanding complex catalytic systems by using a combination of theoretical and experimental techniques.

As shown in Figure 1, isophorone is an  $\alpha,\beta$ -unsaturated cyclic ketone with a variety of functional groups: carbonyl, olefinic double bond, cyclohexene ring, lone methyl group, and twin methyl group. Figure 1 also shows the experimental IR spectrum of isophorone in the gas phase together with 0.3 monolayers (MLs) of isophorone adsorbed on Pd(111) measured at 130 K. The vibrational modes of the adsorbed molecule change significantly with respect to the gas phase. The most intense peak of the isophorone molecule in the gas phase, located at  $1661\text{ cm}^{-1}$ , vanishes upon adsorption, whereas the bands associated with C–H stretching vibrations, located at  $2700\text{--}3000\text{ cm}^{-1}$ , remain largely unperturbed. To understand the modification of the structure of the adsorbed isophorone molecule, we carry out DFT calculations using the FHI-aims all-electron code<sup>9</sup> with the Perdew–Burke–Ernzerhof (PBE) functional.<sup>10</sup> We find that vdW interactions are crucial for the correct description of isophorone adsorbed on Pd(111). For example, the most stable adsorption geometry and the dehydrogenation pathway can be obtained only by taking into account the vdW forces. Therefore, the PBE+vdW method<sup>11</sup> is employed for calculating dispersion interactions. The importance of including vdW interactions for organic molecules on metal surfaces has also been recently demonstrated in literature.<sup>12–14</sup>

**Received:** January 30, 2012

**Accepted:** February 10, 2012

**Published:** February 11, 2012

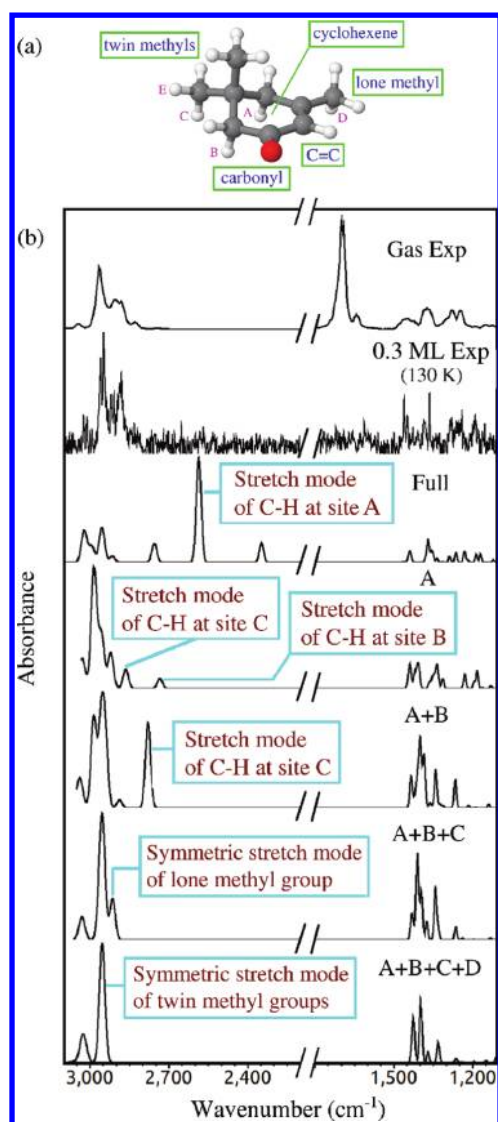


**Figure 1.** (a) Structure of the isolated isophorone molecule. The possible dehydrogenation sites are indicated (sites A–E, see text). (b) Experimental and calculated IR spectra of the intact and dehydrogenated isophorone/Pd(111). (Gas Exp) and (0.3 ML Exp) show the experimental results of the isophorone in the gas phase and on the Pd(111) surface at 130 K, respectively. (Full) depicts the calculated spectrum of  $C_9H_{14}O/Pd(111)$  with Structure I. (A) to (A+B+C+D) show the calculated spectra of the dehydrogenated systems from  $C_9H_{13}O/Pd(111)$  to  $C_9H_{10}O/Pd(111)$ .

We explored the potential-energy surface (PES) of a single isophorone in a  $(4 \times 4)$  supercell by varying the orientation and position of the molecule on top of Pd(111), followed by geometry relaxation. The uppermost two metal layers are allowed to relax, whereas the bottom layers are fixed at their bulk positions. Note that a very large supercell is not necessary for our calculations because the experiments are carried out at moderate coverages. All stable configurations correspond to the oxygen atom, forming a bond with a single Pd atom at the Pd(111) surface. This restricts the complexity of the PES and allows a systematic search for the possible adsorption configurations. We identified five minima that correspond to different tilting angles and lateral positions of isophorone on Pd(111). Figure 2 illustrates the two most stable adsorption structures (S–I and S–II) found in PBE+vdW geometry

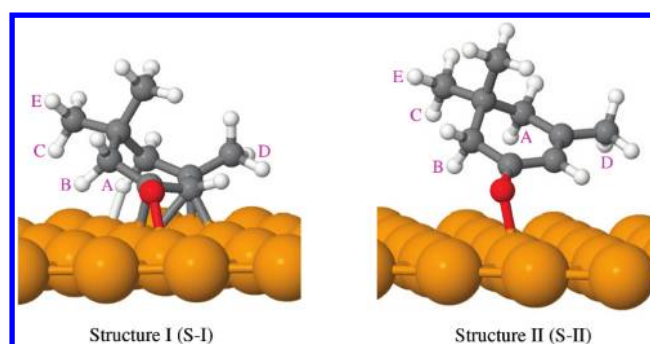


**Figure 2.** Two most stable structures of full isophorone molecule on the Pd(111) surface from the DFT calculations. Structure I is easily obtained by the PBE+vdW method, whereas structure II is mostly located by the PBE functional. The possible dehydrogenation sites are indicated (sites A–E, see text).

relaxations. S–I is significantly closer to the Pd(111) surface than S–II and has three carbon atoms close to the Pd(111) surface. The O–Pd and C–Pd bond lengths (2.14 Å and 2.16 to 2.29 Å, respectively) are similar to typical covalent bond lengths.<sup>15</sup> The bonding arrangement of the S–I structure leads to parallel C=O and C=C bonds with respect to the substrate. The hydrogen atom at site A is also close to a Pd atom (2.07 Å), although at a distance greater than that for solitary hydrogen atoms covalently bonded to hollow sites of Pd(111) (1.80 Å). The adsorption of isophorone induces relaxations of the metal surface. The Pd atoms nearest to the oxygen, carbon, and hydrogen atoms move upward, at most by 0.16 Å, upon adsorption, whereas the remaining metal atoms in the first layer move slightly downward toward the bulk. The changes induced in the second Pd layer are at most 0.05 Å. The geometry of the S–II structure is significantly different. The molecule tilts and forms a  $\sim 40^\circ$  angle with respect to the substrate. Because only one bond is formed between the adsorbate and the substrate, the adsorption energy of S–II (1.24 eV) is weaker than that of S–I (1.79 eV) when using the PBE+vdW method. In contrast, the PBE calculations lack long-range vdW interactions and predict almost equal stability for both structures (0.58 eV for S–I vs 0.42 eV for S–II). Therefore, the inclusion of vdW interactions significantly changes the PES. In fact, S–I was never located by PBE calculations when starting from a random isophorone configuration, whereas S–I was easily obtained using PBE+vdW. Ab initio molecular dynamics (AIMD) simulations further illustrate the difference between PBE and PBE+vdW. We ran a 10 ps trajectory of AIMD at 230 K, starting with S–II. S–II was converted into S–I after 1.7 ps when using PBE+vdW, whereas the molecule desorbed in PBE simulations. Because the desorption of intact isophorone is not observed at 230 K in low coverage TPD experiments, the PBE calculations clearly underestimate the bonding strength. We have also tested the role of screening of vdW interactions inside the Pd bulk by using the combination of PBE+vdW with the Lifshitz–Zaremba–Kohn theory<sup>16</sup> and find adsorption energy differences of  $<0.1$  eV relative to PBE+vdW. This finding is rationalized by the fact that the screening inside the Pd bulk is much smaller than that for the coinage metals (35% reduction in the Pd–Pd  $C_6$  coefficient and 16% reduction in the vdW radius). These two opposing effects lead to a compensation when computing the vdW energy.

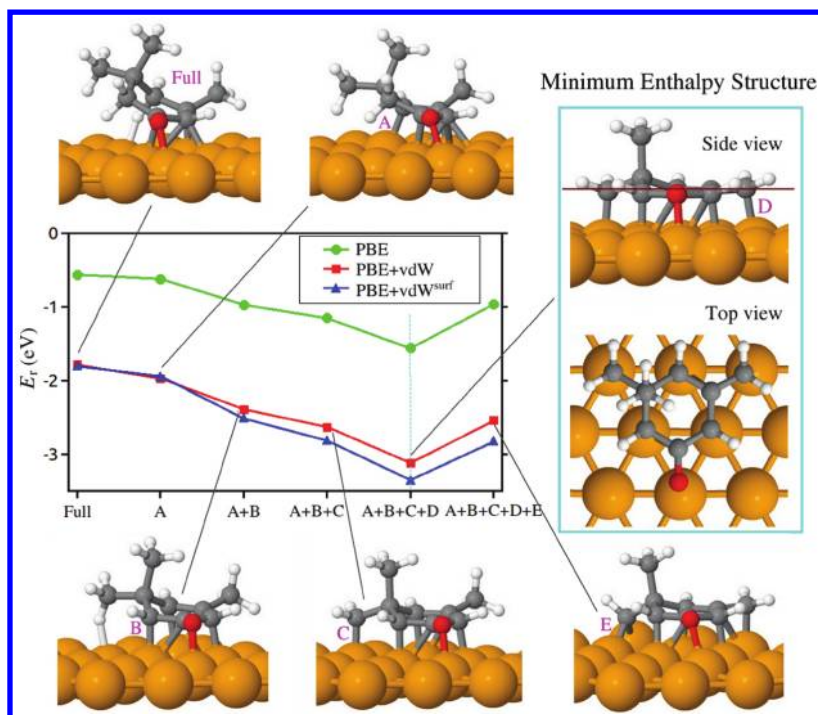


**Figure 3.** Calculated reaction enthalpy  $E_r$  in electronvolts as a function of dehydrogenation step for isophorone/Pd(111). The PBE+vdW<sup>surf</sup> approach includes the screening of the vdW energy in the Pd bulk.<sup>16</sup> The adsorption structure at each step is also shown, where the carbon atom participating in the dehydrogenation is indicated in each plot. The geometry at the minimum enthalpy point (A+B+C+D) corresponds to a flat molecule on the surface.

Owing to the higher stability of S–I, we computed the IR spectrum for this structure using the harmonic approximation (Figure 1, (Full)). The calculated spectrum reproduces the experimentally observed vanishing of carbonyl and C=C (or olefinic) stretching modes that is expected to occur for a flat-lying C=O and C=C bonds with respect to the substrate as a consequence of the metal–surface selection rule.<sup>17</sup> However, there is no qualitative agreement between the calculated and the measured spectra in the high frequency 2200–2900  $\text{cm}^{-1}$  region. The most visible difference appears at 2573  $\text{cm}^{-1}$ , corresponding to the stretch mode of C–H at site A. This discrepancy can arise from substantial broadening of this vibrational band due to a very short lifetime of the C–H–Pd bond precluding its experimental observation. Alternatively, isophorone can decompose by losing the H atom at site A. The latter scenario is very likely on Pd(111), which is known to be active for dehydrogenation reactions.<sup>15,18–20</sup> Furthermore, no mass-spectrum signal corresponding to the intact isophorone molecule was observed in our TPD experiments at low coverage, clearly supporting the dehydrogenation scenario. To explore this possibility and explain the discrepancy between experiments and theory in the IR spectra, we proceed to eliminate the isophorone H atom closest to the Pd(111) substrate (position A in Figure 1). In the low and intermediate coverage limits, which also correspond to the experimental situation, dissociated hydrogen atoms can diffuse on the Pd(111) surface after dehydrogenation occurs, even at low temperatures. The small calculated H diffusion barrier on Pd(111) (0.12 eV, consistent with the literature<sup>21</sup>) confirms

this hypothesis. We thus define the reaction enthalpy of the partially dehydrogenated isophorone molecule,  $E_r$ , as

$$E_r = E_{\text{sys}} + N \times E_{\text{H}/\text{Pd}(111)} - (N + 1) \times E_{\text{Pd}(111)} - E_{\text{mol}} \quad (1)$$

where  $N$  denotes the number of the C–H bond cleavages. The reaction enthalpy is divided into four contributions: (i) the dehydrogenated isophorone on Pd(111),  $E_{\text{sys}}$ ; (ii) a single H atom at the hollow site of Pd(111),  $E_{\text{H}/\text{Pd}(111)}$ ; (iii) the clean Pd(111) surface,  $E_{\text{Pd}(111)}$ ; and (iv) the intact isophorone molecule,  $E_{\text{mol}}$ . Following the first dehydrogenation at site A, we further sequentially remove the hydrogens closest to the substrate, up to five C–H bond cleavages. The calculated  $E_r$  values as a function of the dehydrogenation step are shown in Figure 3. The inclusion of vdW interactions does not affect the calculated trend and results in an increase in the reaction enthalpy. During incremental dehydrogenation steps, the stability consistently increases from the full molecule adsorption (Full) to the fourth dehydrogenation step (A+B+C+D) and then decreases at the fifth step (A+B+C+D+E). We have considered three other possible sites for the fifth dehydrogenation, and none was more stable than site E. The relaxed geometry at the minimum enthalpy structure (A+B+C+D) shows that the entire molecule is flat on the Pd(111) surface and that C–Pd bonds are formed due to the cleavage of the C–H bonds. Note that Figure 3 shows just one of the possible dehydrogenation sequences by “manual” elimination of the H atoms closest to the Pd(111) surface. However, our systematic calculations have confirmed that the fourth step – with these specific four hydrogen atoms extracted – always yields the minimum reaction enthalpy.

The calculated vibrational spectra of the dehydrogenated systems are shown in Figure 1, from the first C–H bond cleavage (A) to the fourth (A+B+C+D). For the initial dehydrogenation, the extremely sharp IR peak, located at  $2573\text{ cm}^{-1}$  in the full-molecule system, vanishes after the first C–H cleavage. However, two small peaks remain in the range of  $2700\text{--}2900\text{ cm}^{-1}$ , corresponding to the stretches of the C–H at sites B and C. After the second dehydrogenation step, as shown in Figure 1 (A+B), an intensive peak appears at  $2772\text{ cm}^{-1}$  due to the stretch mode of the C–H bond at site C, which is not observed in the experimental spectrum. Further removing the third H at site C leads to a qualitative agreement with the experiments. The agreement remains the same after the fourth dehydrogenation step. We conclude based on the IR spectra that multiple (three to four) dehydrogenation steps occur. To gain better understanding of the dehydrogenation kinetics, we use TPD experiments and calculate activation barriers to probe how many C–H bonds break upon adsorption of isophorone on Pd(111).

Decomposition of isophorone was probed by TPD on Pd(111) in the temperature range  $100\text{--}750\text{ K}$  under ultra-high-vacuum conditions. For isophorone coverages in the range of 0.3 to 0.6 ML, no molecular desorption of intact molecule was observed, suggesting complete dissociation of adsorbed species; see Figure 4 (bottom). The strongest signal of intact

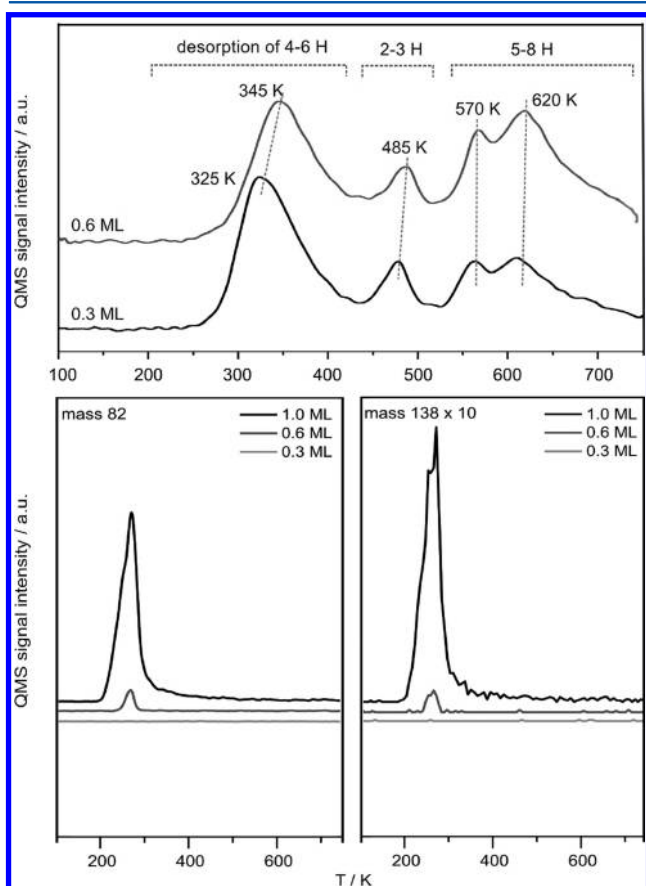


**Figure 4.** Top: TPD spectra obtained after isophorone adsorption at  $100\text{ K}$  on Pd(111) at low (0.3 ML) and intermediate (0.6 ML) coverages. The number of hydrogen atoms desorbing in each peak is estimated from the ratio of the peak areas. Bottom: 82 and 138 amu showing intact isophorone molecules. At low coverage the isophorone decomposes completely on Pd(111).

isophorone molecules (mass 138) is at mass 82, which results from decomposition in the quadrupole mass spectrometer. One of the most prominent desorbing species was  $\text{H}_2$ , which results from isophorone dissociation (see Figure 4). Typically, four distinct desorption peaks at  $320\text{--}350$ ,  $485$ ,  $570$ , and  $620\text{ K}$  can be distinguished. Note that the onset of hydrogen desorption from Pd(111) is well-known to be around  $300\text{ K}$ , which means that the first  $\text{H}_2$  peak is desorption/recombination-limited and that the early decomposition steps contributing to this peak may occur well below  $300\text{ K}$ . All of the subsequent peaks can be undoubtedly attributed to stepwise decompositions at the corresponding temperatures. Assuming that dissociation of each isophorone molecule can release up to the full 14 H atoms, the number of H atoms released in each  $\text{H}_2$  desorption peak was quantified. Before the onset of  $\text{H}_2$  desorption at  $\sim 250\text{ K}$ , four to six H atoms are produced on the surface depending on the ML coverage, where the number six corresponds to the low coverage of 0.3 ML. Because of the coverage used in our calculations (1 molecule per 16 surface atoms,  $\sim 0.5\text{ ML}$ ), the theoretical prediction of four C–H bond cleavages closely matches the TPD result at 0.6 ML. No other molecular decomposition products of isophorone were detected in our experiments at this temperature, which means that the  $\text{H}_2$  trace reflects stepwise decomposition of isophorone and not that of some other molecular surface species. Note that the onset temperature of  $\text{H}_2$  desorption is indicative of recombination of two surface hydrogen atoms,<sup>22</sup> thus the formation of subsurface hydrogen species, which typically desorb from Pd in the range of  $200\text{--}300\text{ K}$ ,<sup>22–24</sup> can be excluded.

To understand further the feasibility of low-temperature dehydrogenation, we proceed to calculate the barriers for the dehydrogenation reaction. The climbing image nudged elastic band (CI-NEB)<sup>25</sup> method was used to determine the activation barrier for dissociation,  $E_a$ . The transition state was characterized by identification of a single imaginary frequency, which corresponds to a saddle point on the PES. Different starting points have been considered for the first C–H cleavage, and site B is found to have the smallest  $E_a$  of  $0.57\text{ eV}$  in PBE+vdW. This value is reduced to  $0.36\text{ eV}$  after including the zero-point energy (ZPE), which is known to play an important role in dehydrogenation reactions.<sup>26,27</sup> The vdW interactions also play a significant role in catalytic reactions.<sup>28</sup> As exemplified in our system, the  $E_a$  value from PBE+vdW is  $\sim 0.1\text{ eV}$  smaller than that from the PBE functional. An even smaller dehydrogenation barrier is found at site A for the second C–H cleavage. In this case,  $E_a$  is determined to be  $0.43\text{ eV}$  without ZPE and reduces to  $0.21\text{ eV}$  with ZPE correction. Our simulations agree with the previous conclusion that the first C–H cleavage is the rate-controlling step during a series of the dehydrogenation reactions.<sup>20</sup>

The calculated barrier of  $0.36\text{ eV}$  for isophorone decomposition corresponds to the temperature range from  $130$  to  $150\text{ K}$ , as estimated by Redhead analysis<sup>29</sup> for the range of preexponential factors  $10^{16}$  to  $10^{13}\text{ s}^{-1}$ , correspondingly, that is typical for large molecules adsorbed on transition metal surfaces.<sup>30–32</sup> The estimated temperature range is in a good agreement with the experimentally observed decomposition below  $\sim 250\text{ K}$ .

In conclusion, a joint theoretical and experimental study is carried out to investigate the structural, vibrational, and catalytic properties of isophorone on the Pd(111) surface. The most stable adsorption geometry can be clearly identified only after the vdW interactions are included in the DFT

calculations. The calculated geometry is in an excellent agreement with the experimental IR spectra, suggesting a flat-lying configuration of the adsorbate. The reaction enthalpy correctly predicts a low-temperature dehydrogenation pathway from the weakly chemisorbed reactant ( $C_9H_{14}O$ ) to the strongly chemisorbed partly dehydrogenation adsorbate ( $C_9H_{10}O$ ). The cleavage of four C–H bonds predicted theoretically is consistent with the TPD results, showing that four to six H atoms can be stripped off below 250 K.

## ■ ASSOCIATED CONTENT

### ● Supporting Information

Experimental details of isophorone adsorbed on the Pd(111) surface. This material is available free of charge via the Internet at <http://pubs.acs.org>.

## ■ AUTHOR INFORMATION

### Corresponding Author

\*E-mail: [tkatchenko@fhi-berlin.mpg.de](mailto:tkatchenko@fhi-berlin.mpg.de); [schauermann@fhi-berlin.mpg.de](mailto:schauermann@fhi-berlin.mpg.de).

### Notes

The authors declare no competing financial interest.

## ■ ACKNOWLEDGMENTS

We are grateful for support from the FP7 Marie Curie Actions of the European Commission, via the Initial Training Network SMALL (MCITN-238804). W.L. was funded by a fellowship from the Alexander von Humboldt Foundation. A.T. acknowledges support from the European Research Council (ERC Starting Grant VDW-CMAT).

## ■ REFERENCES

- (1) Bond, G. C. *Metal-Catalysed Reactions of Hydrocarbons*; Springer Science: New York, 2005.
- (2) Kemball, C. In *Advances in Catalysis and Related Subjects*; Eley, D. D., Selwood, P. W., Weisz, P. B., Eds.; Academic Press: New York, 1959; p 223.
- (3) Somorjai, G. A.; Li, Y. *Introduction to Surface Chemistry and Catalysis*, 2nd ed.; John Wiley & Sons: Hoboken, NJ, 2010.
- (4) Zaera, F. Chiral Modification of Solid Surfaces: A Molecular View. *J. Phys. Chem. C* **2008**, *112*, 16196–16203.
- (5) Doyle, A. M.; Shaikhutdinov, S.; Jackson, S. D.; Freund, H.-J. Hydrogenation on Metal Surfaces: Why are Nanoparticles More Active than Single Crystals? *Angew. Chem., Int. Ed.* **2003**, *42*, 5240–5243.
- (6) Wilde, M.; Fukutani, K.; Ludwig, W.; Brandt, B.; Fischer, J.-H.; Schauermann, S.; Freund, H.-J. Influence of Carbon Deposition on the Hydrogen Distribution in Pd Nanoparticles and Their Reactivity in Olefin Hydrogenation. *Angew. Chem., Int. Ed.* **2008**, *47*, 9289–9293.
- (7) Teschner, D.; Borsodi, J.; Wootsch, A.; Révay, Z.; Hävecker, M.; Knop-Gericke, A.; Jackson, S. D.; Schlögl, R. The Roles of Subsurface Carbon and Hydrogen in Palladium-Catalyzed Alkyne Hydrogenation. *Science* **2008**, *320*, 86–89.
- (8) Beaumont, S. K.; Kyriakou, G.; Watson, D. J.; Vaughan, O. P. H.; Papageorgiou, A. C.; Lambert, R. M. Influence of Adsorption Geometry in the Heterogeneous Enantioselective Catalytic Hydrogenation of a Prototypical Enone. *J. Phys. Chem. C* **2010**, *114*, 15075–15077.
- (9) Blum, V.; Gehrke, R.; Hanke, F.; Havu, P.; Havu, V.; Ren, X.; Reuter, K.; Scheffler, M. Ab Initio Molecular Simulations with Numeric Atom-Centered Orbitals. *Comput. Phys. Commun.* **2009**, *180*, 2175–2196.
- (10) Perdew, J.; Burke, K.; Ernzerhof, M. Generalized Gradient Approximation Made Simple. *Phys. Rev. Lett.* **1996**, *77*, 3865–3868.
- (11) Tkatchenko, A.; Scheffler, M. Accurate Molecular Van Der Waals Interactions from Ground-State Electron Density and Free-Atom Reference Data. *Phys. Rev. Lett.* **2009**, *102*, 073005.
- (12) Stradi, D.; Barja, S.; Díaz, C.; Garnica, M.; Borca, B.; Hinarejos, J. J.; Sánchez-Portal, D.; Alcamí, M.; Arnau, A.; Vázquez de Parga, A. L.; et al. Role of Dispersion Forces in the Structure of Graphene Monolayers on Ru Surfaces. *Phys. Rev. Lett.* **2011**, *106*, 186102.
- (13) McNellis, E.; Meyer, J.; Reuter, K. Azobenzene at Coinage Metal Surfaces: Role of Dispersive Van Der Waals Interactions. *Phys. Rev. B* **2009**, *80*, 205414.
- (14) Atodiresei, N.; Caciuc, V.; Lazić, P.; Blügel, S. Chemical versus Van Der Waals Interaction: The Role of the Heteroatom in the Flat Adsorption of Aromatic Molecules  $C_6H_6$ ,  $C_5NH_5$ , and  $C_4N_2H_4$  on the Cu(110) Surface. *Phys. Rev. Lett.* **2009**, *102*, 136809.
- (15) Jiang, R.; Guo, W.; Li, M.; Lu, X.; Yuan, J.; Shan, H. Dehydrogenation of Methanol on Pd(100): Comparison with the Results of Pd(111). *Phys. Chem. Chem. Phys.* **2010**, *12*, 7794–7803.
- (16) Ruiz, V. G.; Liu, W.; Zojer, E.; Scheffler, M.; Tkatchenko, A. Density-Functional Theory with Screened Van Der Waals Interactions for the Modeling of Hybrid Inorganic/Organic Systems. *Phys. Rev. Lett.* **2012**, accepted.
- (17) Hoffmann, F. M. Infrared Reflection-Absorption Spectroscopy of Adsorbed Molecules. *Surf. Sci. Rep.* **1983**, *3*, 107–192.
- (18) Nilus, N.; Risse, T.; Schauermann, S.; Shaikhutdinov, S.; Sterrer, M.; Freund, H.-J. Model Studies in Catalysis. *Top. Catal.* **2011**, *54*, 4–12.
- (19) Aboul-Gheit, A. K.; Aboul-Fotouh, S. M.; Aboul-Gheit, N. A. K. Hydroconversion of Cyclohexene Using Catalysts Containing Pt, Pd, Ir and Re Supported on H-ZSM-5 Zeolite. *Appl. Catal., A* **2005**, *283*, 157–164.
- (20) Crawford, P.; Burch, R.; Hardacre, C.; Hindle, K. T.; Hu, P.; Kalirai, B.; Rooney, D. W. Understanding the Dehydrogenation Mechanism of Tetrahydrocarbazole over Palladium Using a Combined Experimental and Density Functional Theory Approach. *J. Phys. Chem. C* **2007**, *111*, 6434–6439.
- (21) Watson, G. W.; Wells, R. P. K.; Willock, D. J.; Hutchings, G. J. A Comparison of the Adsorption and Diffusion of Hydrogen on the {111} Surfaces of Ni, Pd, and Pt from Density Functional Theory Calculations. *J. Phys. Chem. B* **2001**, *105*, 4889–4894.
- (22) Christmann, K. Interaction of Hydrogen with Solid Surfaces. *Surf. Sci. Rep.* **1988**, *9*, 1–163.
- (23) Wilde, M.; Fukutani, K.; Naschitzki, M.; Freund, H.-J. Hydrogen Adsorption in Oxide-Supported Palladium Nanocrystals. *Phys. Rev. B* **2008**, *77*, 113412.
- (24) Conrad, H.; Ertl, G.; Latta, E. E. Adsorption of Hydrogen on Palladium Single Crystal Surfaces. *Surf. Sci.* **1974**, *41*, 435–446.
- (25) Henkelman, G.; Uberuaga, B. P.; Jónsson, H. A Climbing Image Nudged Elastic Band Method for Finding Saddle Points and Minimum Energy Paths. *J. Chem. Phys.* **2000**, *113*, 9901.
- (26) Gross, A. *Theoretical Surface Science*; Springer-Verlag: Berlin, 2009.
- (27) Sholl, D. S.; Steckel, J. A. *Density Functional Theory: A Practical Introduction*; John Wiley & Sons: Hoboken, NJ, 2009; p 124.
- (28) Sun, C. Q. Oxidation Electronics: Bond-Band-Barrier Correlation and Its Applications. *Prog. Mater. Sci.* **2003**, *48*, 521–685.
- (29) Redhead, P. A. Thermal Desorption of Gases. *Vacuum* **1962**, *12*, 203–211.
- (30) Tait, S. L.; Dohnálek, Z.; Campbell, C. T.; Kay, B. D. N-Alkanes on MgO(100). II. Chain Length Dependence of Kinetic Desorption Parameters for Small N-Alkanes. *J. Chem. Phys.* **2005**, *122*, 164708.
- (31) Savara, A.; Schmidt, C. M.; Geiger, F. M.; Weitz, E. Adsorption Entropies and Enthalpies and Their Implications for Adsorbate Dynamics. *J. Phys. Chem. C* **2009**, *113*, 2806–2815.
- (32) Zaera, F. Probing Catalytic Reactions at Surfaces. *Prog. Surf. Sci.* **2001**, *69*, 1–98.